FINAL REPORT ON THE

INTEREST JINR University Centre

Wave 6 program

The crystal and magnetic structure of advanced oxide materials: neutron diffraction studies

Supervisor:

Nadezhda Belozerova

Student:

Marija Grujičić, Serbia
"Vinča" Institute of Nuclear Sciences

Participation period:

February 14 – April 01

Dubna, 2022

Abstract

Among nanoparticles based materials, ferrite with spinel structure ($Me^{II}Fe_2O_4$) play very important role in new technological applications, thanks to their chemical and thermal stability, and a rich crystal chemistry that can be exploited for the fine-tuning of the magnetic properties.

The crystal and magnetic structure of spinel $Zn_{0.3}Cu_{0.7}Fe_{1.5}Ga_{0.5}O_4$ has been studied by means of neutron diffraction method. Neutron powder diffraction measurements was performed on the DN-12 diffractometer at the IBR-2 high-flux pulsed reactor (Frank Laboratory of Neutron Physics, Joint Institute for Nuclear Research, Dubna, Russia). Experimental data were analyzed by the Rietveld method using the FullProf software. Spinel $Zn_{0.3}Cu_{0.7}Fe_{1.5}Ga_{0.5}O_4$ belong to the cubic space group $Fd\bar{3}m$. The investigation was held at the wide range of temperatures from 297 K up to 424 K and at the wide range of pressures from 0.8 GPa to 3.4 GPa.

As the result, the crystal and magnetic structures of spinel $Zn_{0.3}Cu_{0.7}Fe_{1.5}Ga_{0.5}O_4$ was defined. Also, lattice parameters, unit cell volume, interatomic bond lengths, bond angles and magnetic moments were observed for each pattern.

Table of contents

Introduction

Among nanoparticles based materials, ferrite with spinel structure ($Me^{II}Fe_2O_4$; $Me^{II} = Fe^{2+}$, Ni^{2+}, Co^{2+}, Cu^{2+}, Zn^{2+}, etc.) play an important role in the quest for new technological applications, thanks to their chemical and thermal stability, and a rich crystal chemistry that can be exploited for the fine tuning of the magnetic properties [1]. Most spinel belong to the cubic space group $Fd\bar{3}m$. Spinel ferrites form a large group of metal oxides in which the trivalent metal ion is Fe^{3+} ion. The diversity of the magnetic properties of spinel ferrites is caused by the peculiar distribution of iron ions between two crystallographic sites [2]. Oxygen anions are densely packed in a surface-centered cubic lattice, while the space between them is filled with cations. Cations occupy two types of positions: tetrahedral (A) and octahedral (B) positions. Cation distribution in spinel structures refers to the distribution of cations between tetrahedral (A) and octahedral (B) positions, so that the structure of spinel ferrites can be described by the general formula:

$$(M^{2+}_{1-\delta}Fe^{3+}_{\delta})_A(M^{2+}_{\delta}Fe^{3+}_{2-\delta})_BO_4, \quad (1)$$

where δ represents the cation distribution factor (degree of inversion) and it shows which part of the tetrahedral sites A is occupied by divalent cations [3]. In relation to the degree of inversion, we distinguish the following spinel structures:

- Normal spinel ($\delta = 0$) - all M^{2+} ions occupy A positions, while Fe^{3+} ions occupy B positions. The structural formula of this type of spinel is $(M^{2+})_A[Fe^{3+}_2]_BO_4$ and this structure is shown by zinc ferrite ($ZnFe_2O_4$),
- Inverse spinel ($\delta = 1$) - all M^{2+} ions occupy B positions, while Fe^{3+} ions are equally distributed between A and B positions. The structural formula of this type of spinel is $(Fe^{3+})_A[M^{2+}Fe^{3+}]_BO_4$ and this structure is shown by cobalt ferrite ($CoFe_2O_4$), nickel ferrite ($NiFe_2O_4$),
- Mixed spinel ($0 \leq \delta \leq 1$) - cation distribution corresponds to that between normal and inverse distribution; the general formula of this type of spinel can be represented by equation (1) [4, 5].

Interconnection between electronic and magnetic properties in the Zn-Cu-Ga ferrites makes this family of ferrites an interesting candidate for exploring the origin and the mechanism of the interplay between structural, electronic and magnetic degrees of freedom in doped spinel

ferrites. Structurally, the interatomic distances and angles can control the strength of the magnetic interactions in spinel-type ferrites [6].

In this work, $Zn_{0.3}Cu_{0.7}Fe_{1.5}Ga_{0.5}O_4$ ferrite was a chosen sample for a neutron diffraction study of the interplay between the crystal and magnetic structures. The neutron diffraction measurements were performed at high pressures form 0.8 GPa to 3.4 GPa and in temperature range 300–424 K.

Properties of $Zn_{0.3}Cu_{0.7}Fe_{1.5}Ga_{0.5}O_4$

The magnetic properties of spinel depend on the magnetic moments of the ions that make up spinel. In ferrites, the main contribution of the magnetic moment comes from the spin moment, while the orbital moment is negligible. Depending on the number of electrons in the outer shell, ions can have different values of total magnetic moment [7, 8]. Since oxygen O^{2-} ions do not have a magnetic moment, the total spinel moment will depend on the magnetic moments of divalent metal ions and trivalent iron ions (or some other trivalent ions, such as gallium). As already mentioned, there are two types of positions that metal cations can occupy and they are tetrahedral (A) and octahedral (B) positions. Néel presented a hypothesis in which the A and B positions are magnetized in opposite directions, which is a consequence of the negative forces of change between the A and B positions in the structure [9]. Moreover, A-B, A-A and B-B interactions tend to be negative, but they cannot be all negative at the same time. These interactions depend on the distance of metal ions from oxygen and the angles between them. A-B interactions are usually the strongest (in A-A or B-B interactions the angles are too small or the distance from oxygen ions is too large), so that all moments at A sites are oriented parallel to each other and antiparallel to those at B sites (Figure 1). However, ions usually do not have the same values of magnetic moments, so they do not cancel each other out and ferrimagnetism occurs - there will be total magnetization [10].

In inverse spinel, such as copper ferrite, iron ions are evenly distributed between A and B sites, so that their magnetic moments cancel each other out and the total magnetization is due to the magnetization of divalent cobalt ions (Cu^{2+}). In the case of zinc ferrite, which is a normal spinel, the situation is a little different. Namely, zinc ions (which occupy A positions) do not have a magnetic moment, so there are no A-B interactions. As a result, B-B interactions can be negative,

so that iron ions (in B places) have antiparallel moments that cancel each other out and the total magnetization is equal to zero. However, B-B interactions are very weak, so zinc ferrite is paramagnetic (it shows antiferromagnetism only at very low temperatures) [9].

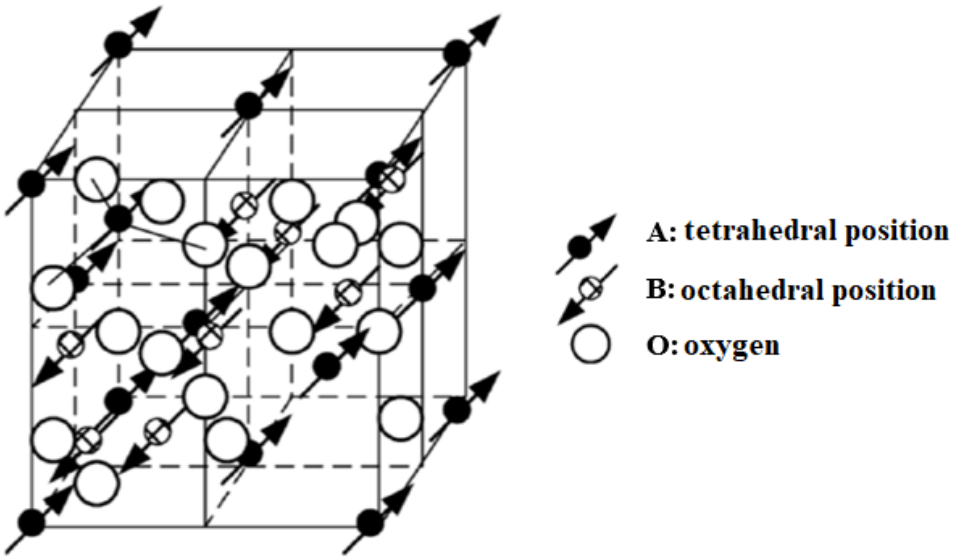

Fig. 1. Schematic representation of the orientation of magnetic moments in the spinel [4]

In Zn-Cu ferrites, the cation-cation [Cu–Cu] and cation-anion-cation [Fe^{3+}–O^{2-}–Fe^{3+}] interactions determine the conductivity of the material. For lower concentrations of zinc ($x < 0.3$), Cu–Cu interaction is dominant, which leads to the behavior of this material as a p-type semiconductor. As the Zn^{2+} concentration increases, the number of Fe^{3+}–O^{2-}–Fe^{3+} interactions increases. On the other hand, Cu-Cu interactions consequently weaken, which leads to the behavior of this material as an n-type semiconductor. The number of Fe^{3+}–O^{2-}–Fe^{3+} bonds determines the magnetic ordering temperatures T_c of ferrite. The incorporation of gallium into the structure, which occupies octahedral positions, reduces the number of Fe^{3+}–O^{2-}–Fe^{3+} bonds and leads to a decrease in T_c [6].

Neutron diffraction

The neutron is a subatomic particle with a neutral charge which was discovered in the first half of the 20th century by James Chadwick. Characteristic properties of neutron scattering are: they interact with the nuclei in the sample, considerable penetration into the depth of the sample, better interaction with lighter atoms, they have spin and they also interact with the magnetic

components in the sample, so it is possible to determine the magnetic arrangement in the sample, the beam of thermal neutrons has wavelengths on the same order of magnitude as the activation energies for many of the solid-state excitations, etc.

The concept of neutron diffraction is opened by W.H.Bragg, W.L.Bragg and Y.V. Wulff and the method is based on reflection of neutrons from some crystal planes when passing through a crystal and on the observation of reflected waves' maximums. The diffraction of thermal neutrons on crystal can be described using Wulff-Bragg' law which is shown in equation (2):

$$2d \cdot \sin\theta = n\lambda \tag{2}$$

where n represents the order of reflection and it must be an integer (n = 1,2, 3…), λ is de Broglie wavelength of neutron $\lambda = \frac{h}{mv} = \frac{h}{p} = \frac{h}{\sqrt{2mE}}$. Any three dimensional periodical crystal can be divided into various sets of equidistant parallel planes and value 'd' represents the distance between two adjacent planes. Angle θ represents an angle of the incident beam and the preferential plane, as it is shown on the Figure 2a. According to Wulff - Bragg's law, constructive interference between the incident and reflected rays occurs when the path between them is equal to the integral multiple of the wavelength. If the total neutron scattering consider as an elastic scattering, the equation that represents Wulff - Bragg's law (2) can be rewritten in another form. In that case, wave vectors of incident and reflected neutrons are equal $|\vec{k}| = |\overrightarrow{k_0}|$, as it is shown on the Figure 2b.

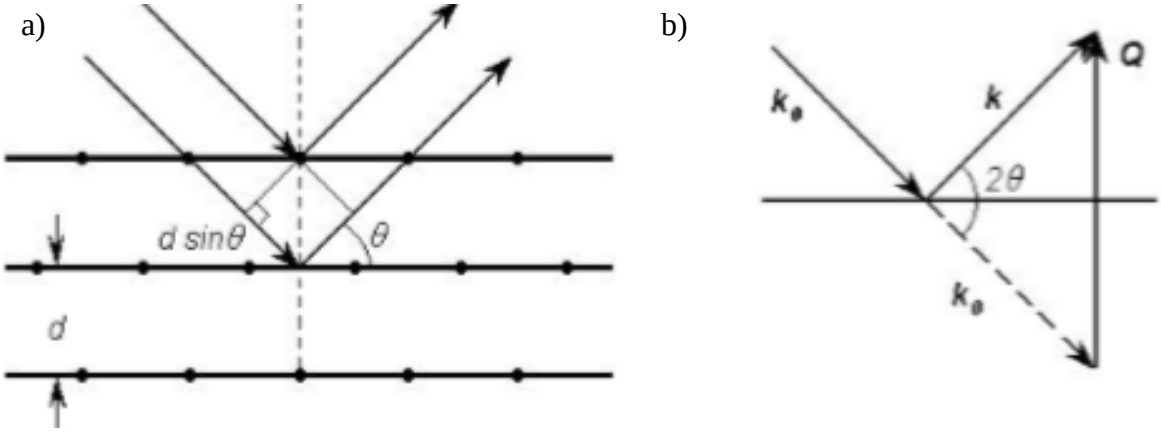

Fig. 2. Bragg reflection from the set of planes with an inter planer spacing of 'd', θ is Bragg angle (a), triangle of neutron scattering (b)

Based on Figure 2b, it can be seen that the scattering wave vector is define as $\vec{Q} = \vec{k} - \overrightarrow{k_0}$ and the diffraction condition can be written as:

$$\vec{\mathrm{Q}} = \left| \vec{k} - \overrightarrow{k_0} \right| = 2\mathrm{k}\sin\theta = 4\pi \cdot \sin\theta/\lambda, \quad (3)$$

where λ represents wavelength of incident neutrons. The distance between two adjacent planes of reciprocal lattice is $d = 1/|\vec{H}|$ and another version of Wulff-Bragg's law can be written as:

$$\delta(\vec{\mathrm{Q}} - 2\pi \cdot n\,\vec{H}). \quad (4)$$

Using Fermi potential it can be described interactions between neutrons and nucleus:

$$V = \frac{2\pi h^2}{m} b \cdot \delta(\vec{r} - \vec{R}), \quad (5)$$

where $\vec{R}$ is a spatial value of the nucleus. Neutron diffraction cross section on the crystal has a new form:

$$\left(\frac{d\sigma}{d\Omega}\right)_{\text{кор}} = \frac{(2\pi)^3}{V_0} \sum_H \delta(\vec{\mathrm{Q}} - 2\pi \cdot n) \cdot |\mathrm{F}(\vec{H})|^2, \quad (6)$$

where V_o is volume of unit cell. Intensity of the diffraction peaks of neutron scattering is proportional to $\left|F(\vec{H})\right|^2$ and they will be observed when the scattering wave vector is actually a vector of the reciprocal lattice:

$$F(H) = \sum_j b_j \exp\left(2\pi \cdot i\vec{H}\vec{r_j}\right), \quad (7)$$

where b_j represents the coherent amplitudes of neutron scattering and $\vec{r_j}$ represents coordinates of atoms in the cell.

Time of flight method (TOF)

Time of flight method (TOF) is one of the common methods of analysis of neutron diffraction. During the long flight path, the neutrons of the sample have some distribution over time, so their energy or wavelength is obtained by measuring this time of flight. In Figure 3 is shown the schema of a TOF diffraction experiment.

The detector signal is stored in a multichannel time analyzer which is started synchronously with each pulse emission. The spectrum represents dependence between recorded counts and neutron flight time [11]. Neutron diffraction patterns, obtained in such way, represent time-

resolved diffraction spectra. The range of wavelengths are widely used on the TOF diffractometers, generally 0,9 – 8 Å.

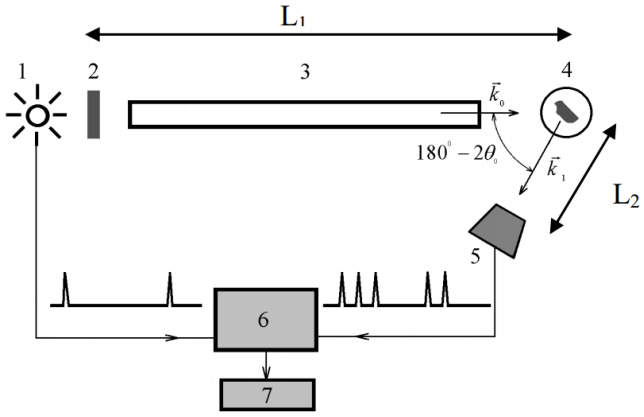

Fig. 3. The lay-out of a TOF diffraction experiment: 1 – pulsed neutron source, 2 – moderator, 3 – flight path of the primary beam, 4 – sample, 5 – detector, 6 – time analyzer, 7 – RW memory

Kinetic moment of neutron, p, can be described by formula:

$$p = mv = \frac{h}{\lambda}, \tag{8}$$

where m is neutron mass and v its velocity. The wavelength of neutron can be described by the Louis de Broglie equation:

$$\lambda = \frac{h}{mv}. \tag{9}$$

From the measurements of flight times of neutrons (t), their velocity is:

$$v = \frac{L_0 - L_1}{t}. \tag{10}$$

Thus, the wavelength of neutron can be written as

$$\lambda = \frac{ht}{m(L_0 + L_1)}. \tag{11}$$

If the crystal planes have Miller indices (hkl) and if θ_0 and λ are fixed, the reflection occurs when Wulff-Bragg's low is fulfilled:

$$2d_{hkl} sin\theta_0 = \lambda \tag{12}$$

The distance between two adjacent planes d_{hkl} should measure up and combining equations (11) and (12) it can be expressed by following equation:

$$d_{hkl} = \frac{ht}{2m(L_0 + L_1) sin\theta_0}. \tag{13}$$

The resolution of the TOF diffractometer is given as:

$$R = \frac{\Delta d}{d} = \left(\left(\frac{\Delta t}{t}\right)^2 + (ctg\theta\Delta\theta)^2\right)^{1/2}, \quad (14)$$

where Δt is equivocation of time of flight and $\Delta\theta$ is geometric equivocation of dispersal process.

The main advantages of TOF diffraction are: ability to conduct measurements in fixed geometry, working in high pressure cells and increase of the factor of using neutrons from the source in comparison with the other neutron methods. On the other side, the main disadvantage is relatively less precision in comparison with the other neutron methods.

Experimental results and discussion

Neutron powder diffraction measurements for $Zn_{0.3}Cu_{0.7}Fe_{1.5}Ga_{0.5}O_4$ ferrite was performed on the DN-12 diffractometer at the IBR-2 high-flux pulsed reactor (Frank Laboratory of Neutron Physics, Joint Institute for Nuclear Research, Dubna, Russia). Diffraction patterns were collected at scattering angle 90° with the resolution Δd/d=0.012 at d=2 Å [6]. Measurements of pressure dependence from 0.8 GPa to very high pressures of 3.4 GPa were performed at ambient temperature. Measurements of temperature was performed from ambient temperatures (297 K) up to 424 K. Experimental data were analyzed by the Rietveld method using the FullProf software. Spinel $Zn_{0.3}Cu_{0.7}Fe_{1.5}Ga_{0.5}O_4$ belong to the cubic space group $Fd\bar{3}m$ [5].

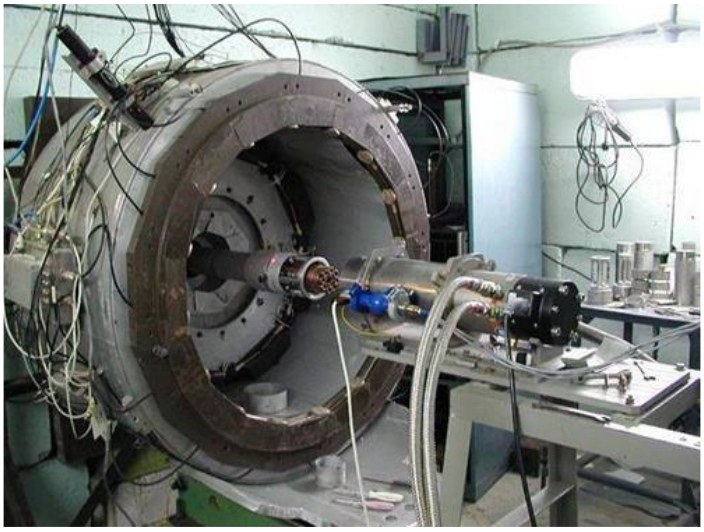

Fig. 4. Photography of DN-12 diffractometer

Temperature dependence measurements

Temperature measurements were performed from 297 K up to higher temperatures of 424 K. At ambient temperature (297 K) spinel $Zn_{0.3}Cu_{0.7}Fe_{1.5}Ga_{0.5}O_4$ has the crystal structure of cubic space group $Fd\bar{3}m$, in which trivalent iron ions Fe^{3+} are distributed between A and B sites [12]. Neutron diffraction patterns of $Zn_{0.3}Cu_{0.7}Fe_{1.5}Ga_{0.5}O_4$ measured at different temperatures are shown in Figure 5.

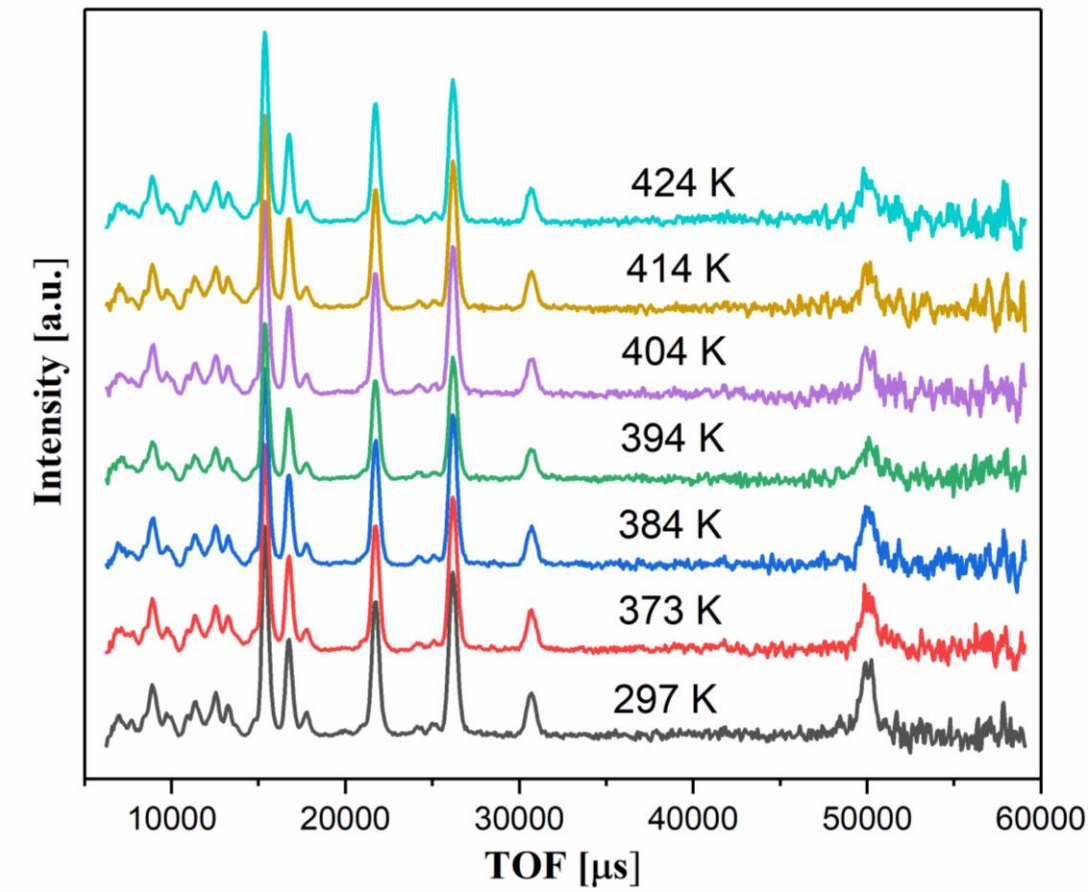

Fig. 5. Neutron diffraction patterns of $Zn_{0.3}Cu_{0.7}Fe_{1.5}Ga_{0.5}O_4$ spinel measured at selected temperatures up to 424 K and processed by the Rietveld method. Experimental points, calculated profiles by the Rietveld method and positions of Bragg peaks are shown

The temperature dependence of the unit cell volume of $Zn_{0.3}Cu_{0.7}Fe_{1.5}Ga_{0.5}O_4$ spinel is shown in Figure 6. Temperature dependences of interatomic bond lengths and angles for the

tetragonal (Fe_A – O) and octahedral (Fe_B – O) oxygen are shown in Figure 7a and Figure 7b, respectively.

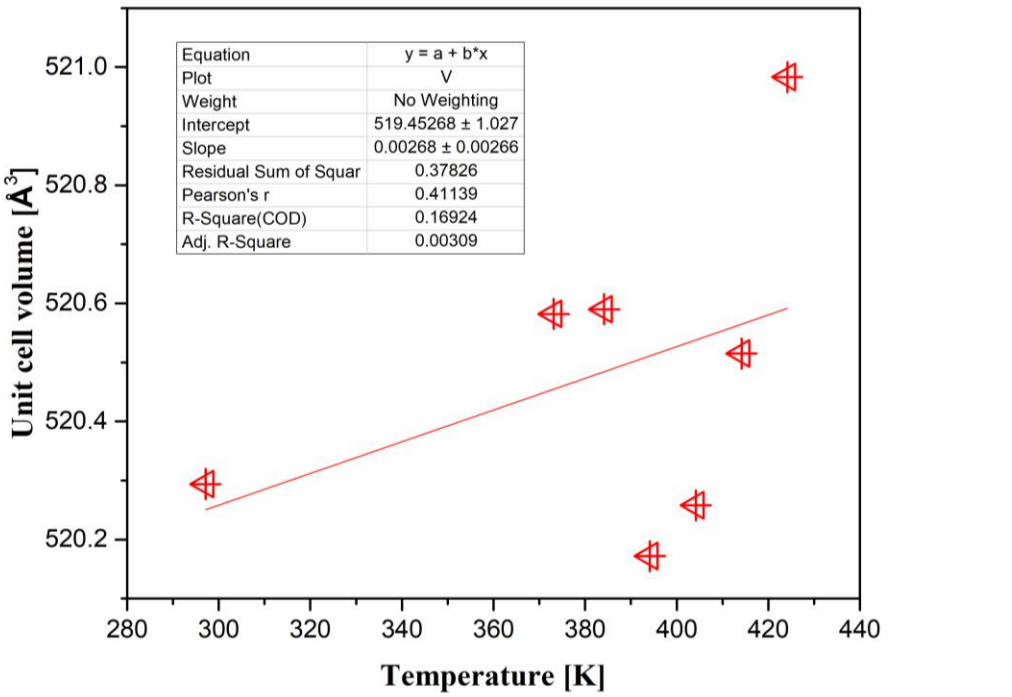

Fig. 6. Temperature dependence of the unit cell volume of $Zn_{0.3}Cu_{0.7}Fe_{1.5}Ga_{0.5}O_4$ spinel. The solid line is linear fit of experimental data.

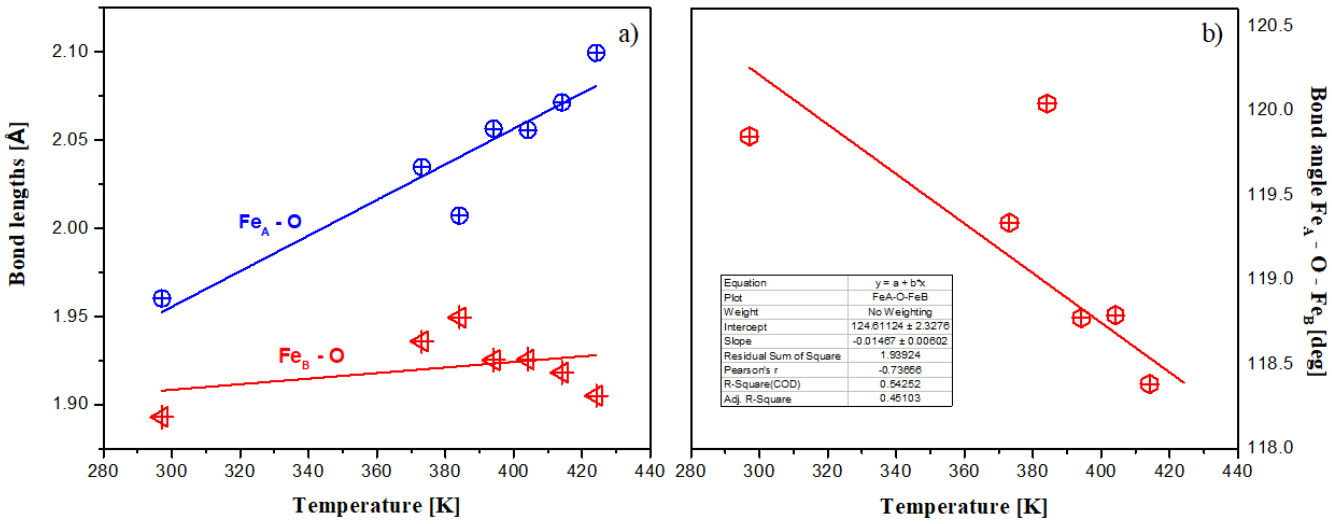

Fig. 7. (a) Fe_A–O and Fe_B–O bond lengths of $Zn_{0.3}Cu_{0.7}Fe_{1.5}Ga_{0.5}O_4$ spinel as a function of temperature. The solid line represents a linear fit to the experimental data. (b) Fe_A–O–Fe_B bond angle of $Zn_{0.3}Cu_{0.7}Fe_{1.5}Ga_{0.5}O_4$ spinel as a function of temperature. The solid line represents a linear fit of the experimental data

By increasing the temperature, Fe_A–O bond length slightly increases. From literature [6] we expected this bond length to decrease. The problem might be in measurements on 295 K temperature, because this value deviates from other values. The Fe_B – O bond length increase with increasing the temperature, which is consistent with the literature [6]. By increasing the temperature, Fe_A–O–Fe_B bond angle decrease (Fig. 7b).

The magnetic moments of the iron ions in different crystallographic sites (A and B) have antiparallel orientation. The temperature dependence of the ordered magnetic moments of Fe in A and B sites are shown in Figure 8. The values of iron magnetics moments are M_A= 3.2(4) μ_B for Fe ions located in tetrahedral sites (A sites) and M_B = 2.6(4) μ_B for those distributed in octahedral (B) sites [9].

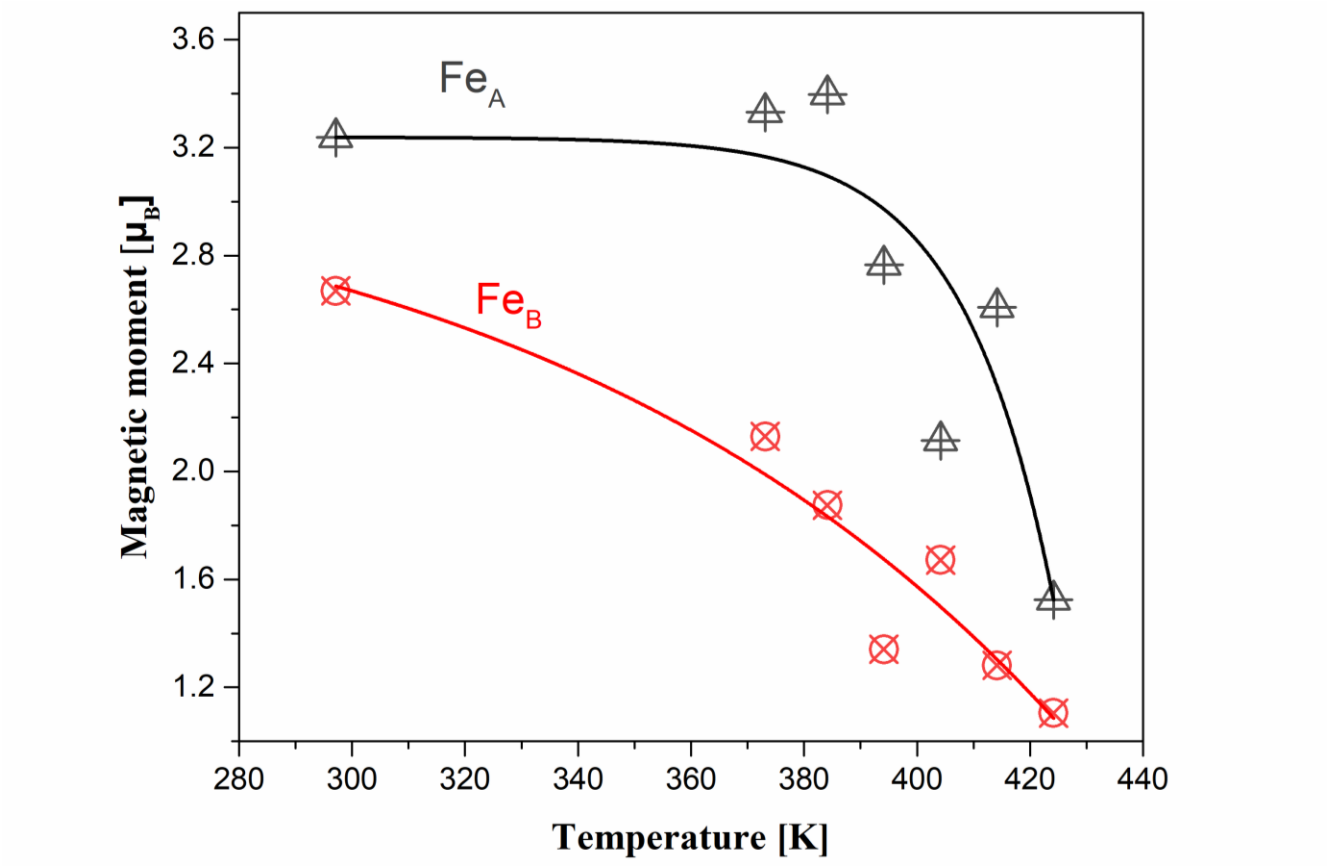

Fig. 8. Temperature dependences of the magnetic moments of iron ions Fe_A and Fe_B located in A and B sites, respectively

Pressure dependence measurements

Pressure measurements were performed from 0.8 GPa up to high pressures of 3.4 GPa at ambient temperature. At ambient temperature (297 K) spinel $Zn_{0.3}Cu_{0.7}Fe_{1.5}Ga_{0.5}O_4$ has the crystal structure of cubic space group $Fd\bar{3}m$, in which trivalent iron ions Fe^{3+} are distributed between A and B sites [12]. Neutron diffraction patterns of $Zn_{0.3}Cu_{0.7}Fe_{1.5}Ga_{0.5}O_4$ measured at different pressures are shown in Figure 9.

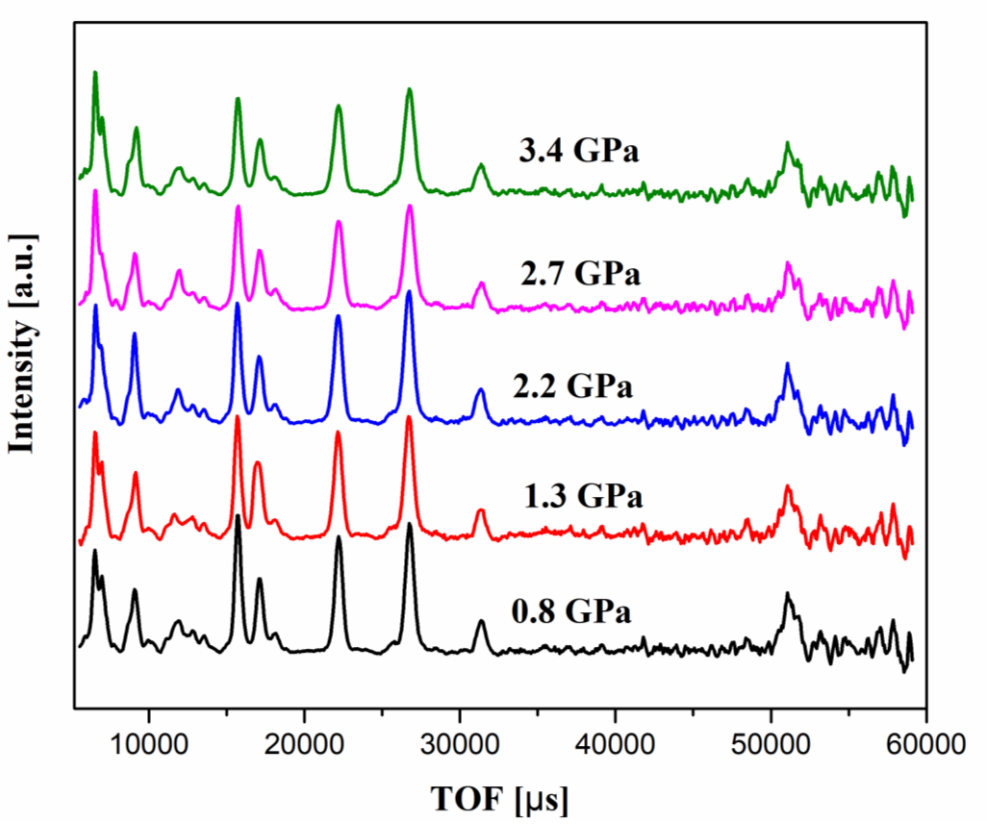

Fig. 9. Neutron diffraction patterns of $Zn_{0.3}Cu_{0.7}Fe_{1.5}Ga_{0.5}O_4$ spinel measured at selected pressures up to 3.4 GPa and processed by the Rietveld method. Experimental points, calculated profiles by the Rietveld method and positions of Bragg peaks are shown

The obtained pressure dependence of the lattice parameter and unit cell volume are shown in Figure 10a and Figure 10b, respectively.

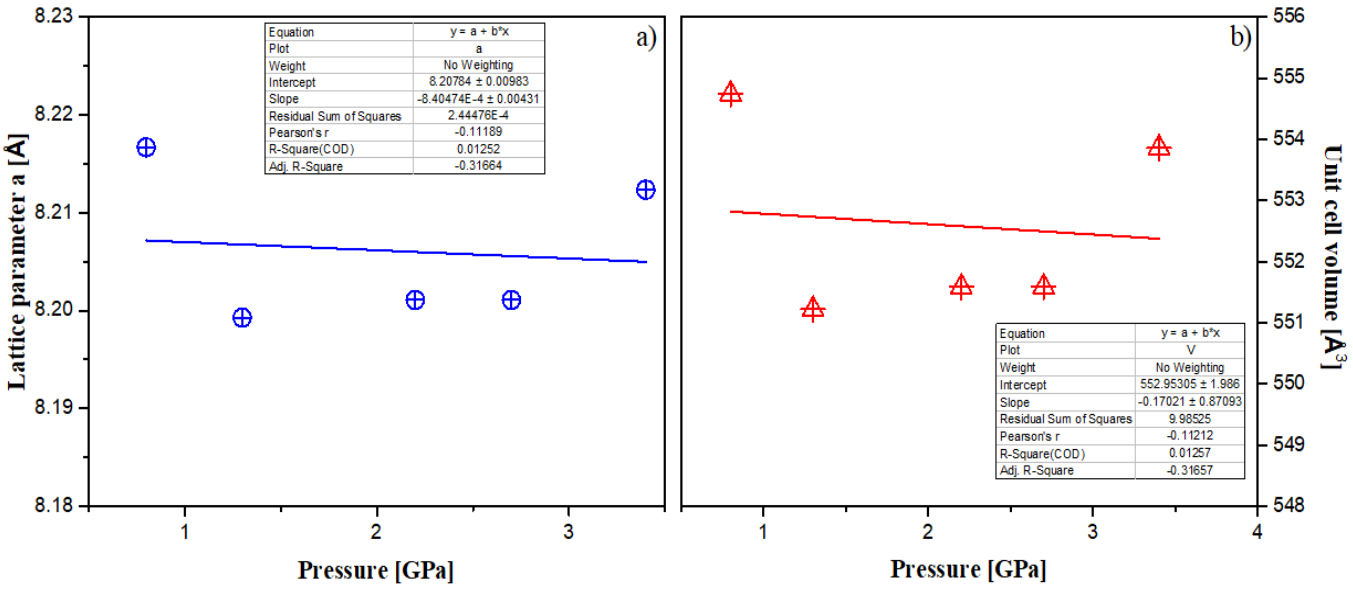

Fig. 10. (a) The pressure dependence of the cubic lattice parameter of $Zn_{0.3}Cu_{0.7}Fe_{1.5}Ga_{0.5}O_4$ spinel. (b) The pressure dependence of unit cell volume of spinel

The pressure dependence of unit cell volume were fitted by the third-order Birch–Murnaghan equation of state [13]:

$$y = \frac{3}{2} \cdot B_0 \cdot \left(x^{-7/3} - x^{-5/3}\right) \cdot \left(1 + \frac{3}{4} \cdot (B_1 - 4) \cdot \left(x^{-2/3} - 1\right)\right), \quad (15)$$

where $x = V/V_0$ is unit cell volume divided by volume at pressure 0 GPa, while B_0 and B_1 are the bulk modulus $B_0 = -V(dP/dV)_T$ and its pressure derivative $B_1 = (dB_0/dP)_T$ [6]. The best fit is achieved by $B_1 = 4$ GPa. The value of bulk module B_0 is 76.3 GPa.

Pressure dependences of interatomic bond lengths for the tetragonal (Fe_A–O) and octahedral (Fe_B–O) oxygen is shown in Figure 11a, while pressure dependences of Fe_A–O–Fe_B bond angle is shown in Figure 11b. By increasing pressure interatomic bond Fe_A – O slightly decrease, while interatomic bond Fe_B – O slightly increase. The Fe_A–O–Fe_B bond angle increase under compression.

The magnetic moments of the iron ions in different crystallographic sites (A and B) have antiparallel orientation. The pressure dependence of the ordered magnetic moments of Fe in A and

B sites are shown in Figure 12. The values of iron magnetics moments are M_A= 3.9(4)μ_B for Fe ions located in tetrahedral sites (A sites) and M_B = 2.8(4)μ_B for those distributed in octahedral (B) sites.

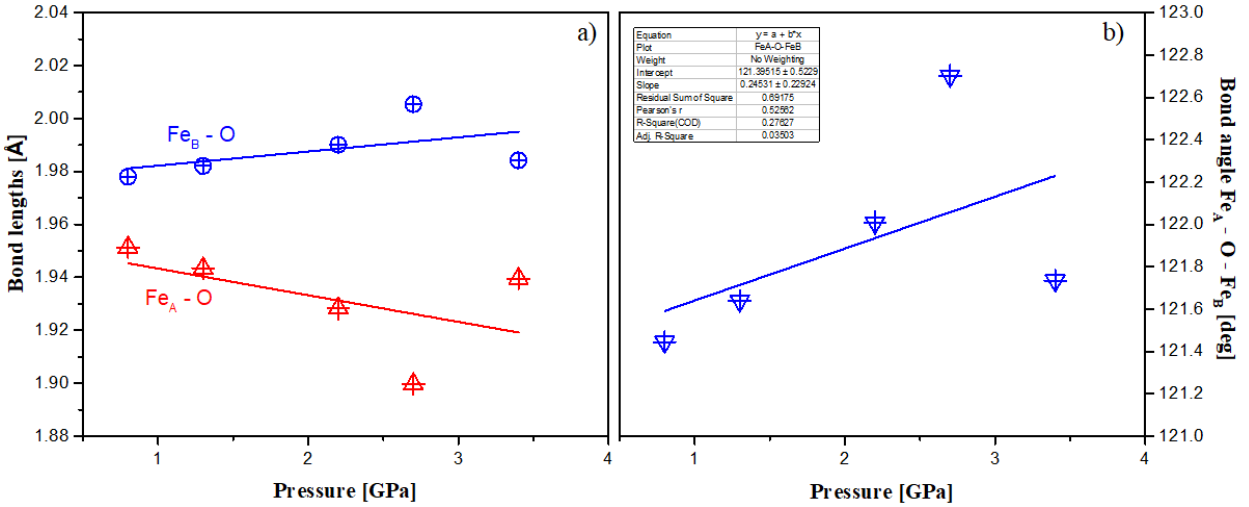

Fig. 11. (a) Fe_A–O and Fe_B–O bond lengths of $Zn_{0.3}Cu_{0.7}Fe_{1.5}Ga_{0.5}O_4$ spinel as a function of pressure. The solid line represents a linear fit to the experimental data. (b) Fe_A–O–Fe_B bond angle of $Zn_{0.3}Cu_{0.7}Fe_{1.5}Ga_{0.5}O_4$ spinel as a function of pressure. The solid line represents a linear fit of the experimental data

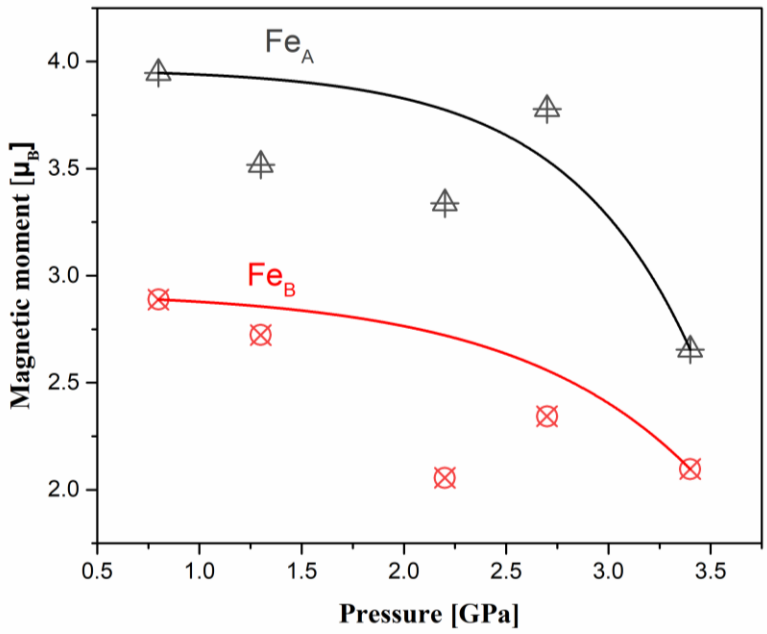

Fig. 12. Pressure dependences of the magnetic moments of iron ions Fe_A and Fe_B located in A and B sites, respectively

Conclusion

The structural and magnetic properties of spinel ferrite $Zn_{0.3}Cu_{0.7}Fe_{1.5}Ga_{0.5}O_4$ have been studied by means of the neutron diffraction method at pressures from 0.8 GPa to high pressures of 3.4 GPa and in temperature range 297–425 K. Experimental data were analyzed by the Rietveld method using the FullProf software. Spinel $Zn_{0.3}Cu_{0.7}Fe_{1.5}Ga_{0.5}O_4$ belong to the cubic space group $Fd\bar{3}m$.

By increasing the temperature, Fe_A–O and Fe_B – O bond lengths both increases. By increasing the temperature, Fe_A–O–Fe_B bond angle decrease. The magnetic moments of the iron ions in different crystallographic sites (A and B) have antiparallel orientation. The values of iron magnetics moments are M_A= 3.2(4) μ_B for Fe ions located in tetrahedral sites (A sites) and M_B = 2.6(4) μ_B for those distributed in octahedral (B) sites.

The best fit of dependence between pressure and unit cell volume was achieved when bulk modules was B_1= 4 GPa and B_0=76.3 GPa. By increasing pressure interatomic bond Fe_A – O slightly decrease, while interatomic bond Fe_B–O slightly increase, while the Fe_A–O–Fe_B bond angle increase under compression. The values of iron magnetics moments are M_A= 3.9(4) μ_B for Fe ions located in tetrahedral sites (A sites) and M_B = 2.8(4) μ_B for those distributed in octahedral (B) sites.

Acknowledgement

I take this opportunity to express my profound gratitude and kind regards to my supervisor N. M. Belozerova for her guidance, monitoring and constant encouragement throughout the course of this project.

Also, I would like to thank a committee of JINR Student Program for opportunity to participate in this program.

References

[1] Muscas G, Jovanović S, Vukomanović M, Spreitzer M, Peddis D, Zn-doped cobalt ferrite: Tuning the interactions by chemical composition, *Journal of Alloys and Compounds,* Vol. 796, No. pp. 203-209, 2019.

[2] Gubin S, Koksharov Y, Khomutov G, Yurkov G, Magnetic nanoparticles: Preparation, structure and properties, *Russian Chemical Reviews,* Vol. 74, No. pp. 539-574, 2005.

[3] Sickafus KE, Wills JM, Grimes NW, Structure of Spinel, *Journal of the American Ceramic Society,* Vol. 82, No. 12, pp. 3279-3292, 1999.

[4] Mathew DS, Juang R-S, An overview of the structure and magnetism of spinel ferrite nanoparticles and their synthesis in microemulsions, *Chemical Engineering Journal,* Vol. 129, No. 1, pp. 51-65, 2007.

[5] Milanović M, Sinteza i karakterizacija nanočestičnih prahova na bazi cink-ferita, *Универзитет у Новом Саду,* Vol. No. pp. 2010.

[6] Kozlenko D, Belozerova N, Ata-Allah S, Kichanov S, Yehia M, Hashhash A, Lukin E, Savenko B, Neutron diffraction study of the pressure and temperature dependence of the crystal and magnetic structures of Zn0. 3Cu0. 7Fe1. 5Ga0. 5O4 polycrystalline ferrite, *Journal of Magnetism and Magnetic Materials,* Vol. 449, No. pp. 44-48, 2018.

[7] Smit J, Wijn H, Ferrites, Philips technical library, *Eindhoven, The Netherlands,* Vol. 278, No. pp. 1959.

[8] Jovanović S, Spreitzer M, Otoničar M, Jeon J-H, Suvorov D, pH control of magnetic properties in precipitation-hydrothermal-derived CoFe2O4, *Journal of alloys and compounds,* Vol. 589, No. pp. 271-277, 2014.

[9] Cullity BD, Graham CD. *Introduction to magnetic materials,* John Wiley & Sons, 2011.

[10] Goldman A. *Modern ferrite technology,* Springer Science & Business Media, 2006.

[11] Johnson MG, Giacomelli L, Hjalmarsson A, Källne J, Weiszflog M, Sundén EA, Conroy S, Ericsson G, Hellesen C, Ronchi E, The 2.5-MeV neutron time-of-flight spectrometer TOFOR for experiments at JET, *Nuclear Instruments and Methods in Physics Research Section A: Accelerators, Spectrometers, Detectors and Associated Equipment,* Vol. 591, No. 2, pp. 417-430, 2008.

[12] Chinnasamy C, Narayanasamy A, Ponpandian N, Chattopadhyay K, Shinoda K, Jeyadevan B, Tohji K, Nakatsuka K, Furubayashi T, Nakatani I, Mixed spinel structure in nanocrystalline NiFe 2 O 4, *Physical Review B,* Vol. 63, No. 18, pp. 184108, 2001.

[13] Greenberg E, Rozenberg GK, Xu W, Arielly R, Pasternak M, Melchior A, Garbarino G, Dubrovinsky L, On the compressibility of ferrite spinels: a high-pressure X-ray diffraction study of M Fe2O4 (M= Mg, Co, Zn), *High Pressure Research,* Vol. 29, No. 4, pp. 764-779, 2009.